Global and Planetary Change 233 (2024) 104365

Contents lists available at ScienceDirect

Global and Planetary Change

journal homepage: www.elsevier.com/locate/gloplacha

Enhanced primary productivity and perturbation of marine nitrogen cycling during the onset of the Cambrian SPICE event

Gwen L. Barnes [a,b,*], Bradley D. Cramer [a]

[a] Department of Earth and Environmental Sciences, University of Iowa, Iowa City, IA 52242, USA
[b] Department of Earth, Atmospheric, and Ocean Sciences, Florida State University, Tallahassee, FL 32306, USA

ARTICLE INFO

Keywords:
Cambrian
SPICE
Nitrogen isotopes
Marine redox
Nutrient cycling

ABSTRACT

New high-resolution paired carbonate carbon ($\delta^{13}C_{carb}$) and nitrogen ($\delta^{15}N_{bulk}$) isotope records of the Steptoean Positive Carbon Isotope Excursion (SPICE) from the Laurentian epicontinental platform reveal a transient negative excursion in $\delta^{15}N_{bulk}$ that closely aligns with the onset of the SPICE event and the initiation of the positive $\delta^{13}C_{carb}$ excursion. The negative excursion in $\delta^{15}N_{bulk}$ identified here likely demonstrates an increase in microbially fixed nitrogen by diazotrophs, or cyanobacteria capable of N_2 fixation, in the marine system due to a reduction in bioavailable recycled N through several processes at the onset of the biogeochemical event. Expansion of reducing environments during the initiation of the SPICE event would have liberated phosphorous previously bound to organic matter and/or marine iron oxy-hydroxides and simultaneously promoted an expansion of denitrification in oxygen-poor settings that would have reduced bioavailable N in the marine system. The enhanced delivery of phosphorous to the photic zone would have stimulated primary productivity, which would have also put additional pressure on the marine bioavailable N budget. These feedback systems would have combined to lower the marine N:P ratio such that diazotrophs would become a significant contributor to the total bioavailable N in the marine realm. The data presented here are the first demonstration of this significant perturbation to local marine nutrient cycling during the onset of the SPICE event and provide new insight into what may ultimately be a consistent set of biogeochemical triggers for major Paleozoic biogeochemical events.

1. Introduction

Perturbations to the global carbon cycle are reflected in the carbon isotope composition ($\delta^{13}C$) of the ocean-atmosphere system and are then preserved in the stratigraphic record as pronounced transient variations in $\delta^{13}C$ values. These "excursions" in the $\delta^{13}C$ record represent periods of disequilibrium in the cycling of carbon between the linked atmospheric, oceanic, biological, and sedimentary reservoirs (Hayes et al., 1999; Cramer and Jarvis, 2020). Closely examining such events that punctuate Earth history provide significant insight into the evolution of the atmosphere-ocean-biosphere system and, in particular, the influence that biogeochemical cycling of nutrients plays in the global carbon cycle via their influence on marine primary productivity.

The Cambrian Period (~539–487 Ma) marks the transition from the highly unstable, volatile $\delta^{13}C$ record of the Neoproterozoic to the increasingly more stable Paleozoic $\delta^{13}C$ record (Bachan et al., 2017; Cramer and Jarvis, 2020). At least ten major perturbations to the global carbon cycle punctuate the Cambrian (Zhu et al., 2019; Cramer and Jarvis, 2020), and the Steptoean Positive Carbon Isotope Excursion (SPICE) was the final major positive excursion of this period and is characterized by a + 3‰ to +6‰ shift (absolute magnitude of change) in carbonate carbon isotope values ($\delta^{13}C_{carb}$). The onset of the SPICE coincides with the base of the Paibian Stage (~495 Ma) of the Furongian Series, and the event persisted for approximately the next 2–3 million years (Saltzman et al., 2000; Cothren et al., 2022; Zhao et al., 2022). In Laurentia, the rising limb of this excursion tracks falling sea level associated with the Sauk II-III subsequence boundary with maximum $\delta^{13}C_{carb}$ values occurring somewhere near the height of regression (Runkel et al., 1998; Saltzman et al., 2000). A global turnover of trilobites at the Laurentian Marjumiid-Pterocephaliid biomere boundary (As first defined by Palmer, 1965, "biomere" refers to a trilobite-based, extinction-bounded biostratigraphic unit exclusive to Laurentia; e.g., Palmer, 1984; Taylor, 2006) and in stratigraphically equivalent Gondwanan sections also corresponds to the beginning of the SPICE

* Corresponding author.
E-mail addresses: gwen-barnes@uiowa.edu, gb23@fsu.edu (G.L. Barnes).

https://doi.org/10.1016/j.gloplacha.2024.104365
Received 6 June 2023; Received in revised form 8 January 2024; Accepted 12 January 2024
Available online 15 January 2024

(Saltzman et al., 2000; Zhang et al., 2023).

The SPICE event has been documented globally (Zhang et al., 2023) in numerous depositional settings across Laurentia (Saltzman et al., 2004; Schiffbauer et al., 2017; LeRoy and Gill, 2019), Baltica (Ahlberg et al., 2019), Avalonia (Woods et al., 2011), Siberia (Kouchinsky et al., 2008), Kazakhstan (Saltzman et al., 2000), and Gondwana (Schmid et al., 2018; LeRoy et al., 2021) and is thus interpreted to be an expression of a major biogeochemical perturbation that included significant changes in biological communities, the global carbon and sulfur cycles, and the biogeochemical cycling of major- and trace-elements in the ocean-atmosphere-biosphere system (Zhang et al., 2023; Zhao et al., 2023). Though most published studies focus on the $\delta^{13}C_{carb}$ record, a handful of studies additionally recognized positive excursions in the organic carbon isotope record ($\delta^{13}C_{org}$; Saltzman et al., 2011; Woods et al., 2011; Ahlberg et al., 2019; Li et al., 2018). Coeval positive excursions in the isotopic values of sulfur in carbonate-associated sulfate and pyrite have also been identified in sections from Laurentia, Baltica, Gondwana, Avalonia, and Australia (Gill et al., 2011; LeRoy et al., 2021; Zhang et al., 2023). Investigations of redox and biogeochemical cycling of elements using various other geochemical proxies (e.g., molybdenum, uranium, mercury, iron, neodymium) reveal notable deviations from baseline values as well (Gill et al., 2011, 2021; Dahl et al., 2014; Pruss et al., 2019; LeRoy et al., 2021; Rooney et al., 2022; Zhao et al., 2023). While the precise driving mechanisms of the SPICE are still debated, these signals are most commonly interpreted to represent an episode of expanding reduced marine environments (anoxia/euxinia) and the consequent enhancement of organic carbon burial in the marine realm.

Whereas the consequences of the SPICE event (biotic turnover, expansion of reducing environments, enhanced organic carbon burial) have been well documented, fundamental questions remain regarding the ultimate triggers of the event (e.g., Rooney et al., 2022) and, in particular, the combined roles that changes in biogeochemical nutrient cycling and primary productivity may have played in the initiation of this event. Nitrogen is an essential nutrient for marine phytoplankton, and the availability of bioavailable N substantially impacts primary production in the modern ocean. The history of the marine nitrogen cycle has been largely unexplored for much of the Cambrian, and the $\delta^{15}N$ record of the SPICE event is generally unknown (Hammer and Svensen, 2017). Here, we examine changes in the marine N cycle during the SPICE event by producing paired high-resolution records of $\delta^{13}C_{carb}$ and $\delta^{15}N_{bulk}$ from the SPICE in a core from central Iowa to investigate the relationship between nutrient cycling, primary productivity, and organic carbon burial. The isotopic record of marine nitrogen is largely dependent on local nutrient availability (e.g., N:P) and changes in redox conditions in the oceans, thereby making the record necessarily a highly local signal. This study takes the first step in documenting high-resolution changes in the marine nitrogen cycle during the initiation of the SPICE event.

2. The marine nitrogen cycle

Nitrogen is one of the most significant bio-limiting nutrients for marine phytoplankton and plays a critical role in controlling the location, type, and amount of primary production in the oceans (e.g., Gruber and Sarmiento, 1997; Tyrrell, 1999; Gruber and Galloway, 2008; Hutchins and Capone, 2022). Though abundant as an atmospheric gas, N_2 is not biologically useful for most species. The triple bonds of N_2 must be broken and the N "fixed" to a bioavailable form in order for the nutrient N to be accessible to and utilized by most organisms. Marine nitrogen fixation is typically carried out by cyanobacterial diazotrophs who convert molecular nitrogen (N_2) to ammonia (NH_3) in the surface ocean, but some non-cyanobacterial diazotrophic (NCD) fixation of nitrogen occurs below the surface ocean as well (Hutchins and Capone, 2022). Under oxic conditions, nitrification then converts reduced nitrogen in NH_3 to nitrite (NO_2^-) and then to fully oxidized nitrate (NO_3^-). These processes play the dominant roles, along with recycling of organically-bound N into NH_4^+ during organic matter remineralization in reducing environments, in providing the bioavailable N to marine phytoplankton (e.g., Voss et al., 2013; Hutchins and Capone, 2022). Together, NO_3^- and NH_4^+ comprise the fixed nitrogen inventory of the ocean for most phytoplankton. In addition to biotic assimilation of fixed nitrogen into organic matter, the loss of fixed N typically takes place below the photic zone in suboxic to anoxic conditions dominantly through denitrification (stepwise reduction of NO_3^- to N_2 gas) and the anaerobic oxidation of ammonia (anammox; oxidation of NH_4^+ with NO_2^- to N_2). Dissimilatory nitrate reduction to ammonia (DNRA) in oxygen minimum zones (OMZs) or anoxic sediments and deamination (converting organic N back into NH_3) also serve to reduce the marine fixed nitrogen inventory.

Two stable isotopes of nitrogen exist, ^{14}N and ^{15}N, and as with most other isotope systems, biological, chemical, and physical processes impart a variety of fractionations on the global nitrogen isotope system (e.g., Gruber, 2004). The effects of fractionation driven by net changes between sources and sinks are reflected as changes in the ratio of ^{15}N to ^{14}N relative to a standard (air), typically reported as $\delta^{15}N$ ($\delta^{15}N_{bulk}$ for most whole-rock N-isotope data in deep-time geologic studies), and the discrimination between these two isotopes of nitrogen also means that $\delta^{15}N$ varies between nitrogen pools (e.g., atmosphere, ocean, organic matter, and marine sediments). Atmospheric N_2 ($\delta^{15}N_{air}$) carries a $\delta^{15}N$ signature of 0‰, and the "average" $\delta^{15}N$ of modern seawater is around +5‰ (Sigman and Casciotti, 2001; Gruber, 2004). Nitrogen fixation of N_2 to NH_3 by marine diazotrophs and nitrification to NO_3^- produces nutrient N with low $\delta^{15}N$, usually close to 0‰ (Gruber, 2004). The N-isotopic composition of marine sediments is largely driven by the N-isotopic composition of the oceans through biological uptake of N, meaning that the isotopic signature of sediments will typically change if the isotopic value of the main source of bioavailable nitrogen in overlying waters changes. For example, the $\delta^{15}N$ of sediments will typically decrease if nitrogen fixation by diazotrophs is the main source of bioavailable nitrogen in the overlying water column (e.g., Kuypers et al., 2004; Liu et al., 2015) or if organic matter remineralization in reducing conditions leads to an increase in the relative importance of NH_4^+ to the overall bioavailable local N budget (Junium and Arthur, 2007; Higgins et al., 2012; Ruvalcaba Baroni et al., 2015). The global mean nitrogen cycle can be very different from the cycling of nitrogen occurring in specific environments given the largely biologically mediated nature of the nitrogen cycle, and the relative interactions between sources (marine nitrogen fixation) and sinks (denitrification/anammox/DNRA) are the drivers of transient changes in local N-isotope signals (Gruber, 2004; Liu et al., 2015). Ultimately, marine environments with low $\delta^{15}N$ values (near or below 0‰) are most frequently interpreted to reflect an environment dominated by either nitrogen fixation, assimilation of NH_4^+, or some combination thereof (e.g., Kuypers et al., 2004; Junium and Arthur, 2007; Higgins et al., 2012; Liu et al., 2015; Ruvalcaba Baroni et al., 2015; Naafs et al., 2019).

The classical negative feedbacks between net changes in denitrification in reducing environments and the competitive advantages bestowed upon nitrogen fixers under decreasing N:P dominate our understanding of the modern oceanic N inventory through regulation by this "Nitrostat" (Van Cappellen and Ingall, 1994; Falkowski et al., 1998; Tyrrell, 1999; Lenton and Watson, 2000; Saltzman, 2005; Gruber and Galloway, 2008; Moore et al., 2013; Voss et al., 2013). Whereas P is increasingly remobilized from both iron oxy-hydroxides and organic matter during expansion of reducing environments, NO_3^- is increasingly denitrified and removed from the marine fixed N inventory, thus driving lower N:*P* values and favoring diazotrophy. However, important additions to the classical Nitrostat have also begun to expand our understanding of marine N cycling in the ancient Earth system during conditions with significant differences in atmospheric O_2 and CO_2 concentrations, oceanography, and/or evolutionary development compared to the modern (e.g., Junium and Arthur, 2007; Higgins et al., 2012; Ruvalcaba Baroni et al., 2015; Naafs et al., 2019).

The marine N cycle likely operated very differently during Oceanic Anoxic Events (OAEs) as well as prior to the development of a fully oxygenated atmosphere and ocean. During intervals of significantly diminished marine oxygenation compared to the modern, reducing environments were likely extensive enough in the global oceans to change the redox balance between NO_3^- and NH_4^+ to a point where ammonium became the largest reservoir of fixed N in the oceans and a significant contributor of nutrient N to total organic export production (>20%, Naafs et al., 2019). While NH_4^+ becomes a major reservoir in the global fixed N inventory under such reducing conditions, NH_4^+ assimilation would still not become the dominant source of nutrient N for global export production because most NH_4^+ is nitrified in oxygenated waters immediately underlying the photic zone. NH_4^+ assimilation is typically restricted to locations where the OMZ intersects the photic zone (e.g., Konovalov et al., 2000; Naafs et al., 2019).

3. Geological setting

Shallow marine seas slowly began encroaching onto the North American craton near the end of the Proterozoic during the transgression associated with the Sauk Megasequence, inundating much of Laurentia by the end of the Cambrian (Runkel et al., 1998; Haq and Schutter, 2008). Most of Laurentia was situated between the equator and 30°S (Fig. 1A), which created a broad, tropical epicontinental sea across the continent. In the Upper Mississippi Valley, a combination of gradual uplift along the Transcontinental Arch and rising sea level contributed to the further development of a tectonically stable cratonic shelf known as the Hollandale Embayment (Runkel et al., 1998; Runkel et al., 2012) that extended northward from the Illinois Basin into much of the present-day central Midwest (Fig. 1B). By the middle of the Cambrian Period, this embayment functioned as the primary region for the deposition of Upper Mississippi Valley sediments.

The Upper Mississippi Valley shelf (including the Hollandale Embayment) subsided at a relatively slow rate (<10 m/Myr), had a low gradient (0.1 m/km), and lacked a shelf break into deeper waters (Sloss, 1988; Runkel et al., 1998). The Transcontinental Arch and the Wisconsin Arch and Dome complex bordered the embayment to the west and east, respectively (Runkel et al., 1998, 2007). Proximity to these clastic sources ultimately divided embayment sediments into two laterally adjacent facies belts: a proximal inner detrital belt of shallow siliciclastics and a more distal middle carbonate belt of carbonates and marls (Fig. 1). Much of Iowa, including the Rhinehart A-1 drill core studied here, was located in the middle carbonate belt of the tectonically stable interior of the Hollandale Embayment (Fig. 2). This core was originally drilled in Dallas County, Iowa (41.703323°N, 94.00199°W), and is archived by the Iowa Geological Survey (W#23289) (Figs. 1 & 2).

Well-defined trilobite zones serve as the primary basis for chronostratigraphic correlation between Laurentian rock units of the later part of the Cambrian. In this study, we focus on the Bonneterre and Davis formations, which contain the *Crepicephalus, Aphelaspis, Dunderbergia,* and *Elvinia* zones (Fig. 3; Runkel et al., 1998; Peng et al., 2020). The Bonneterre and Davis formations consist largely of limestones, dolostones, and comparatively more distal marls. The lower part of the Boneterre Formation is composed mainly of gray intraclastic wackestones with occasional glauconite. Strata at the top of the Bonneterre Formation contain abundant glauconite, hematite, and limonite. The lower part of the Davis Formation is characterized by increased occurrences of thicker packstone and grainstone packages, whereas the upper Davis Formation consists of gray calcareous shales with interbedded limestones.

Sea level was at a highstand during the early *Crepicephalus* zone and fell through the *Aphelaspis* and *Dunderbergia* zones (Fig. 3; Runkel et al., 1998). Shorelines prograded from southern Minnesota, Wisconsin, and northern Iowa and reached their maximum basinward positions near the top of the *Dunderbergia* Zone and early *Elvinia* Zone, marking the Sauk II-III subsequence boundary within the global Paibian Stage (Runkel et al., 1998; Saltzman et al., 2004; Peng et al., 2020). This lowstand is marked by the appearance of cratonic sandstone sheets (the Wonewoc Sandstone) in the more proximal regions of the inner detrital belt and is consistent with the packstone and grainstone packages in the carbonate belt.

The location of the Sauk II-III boundary in the Rhinehart A-1 core is difficult to precisely locate due to the distal position of the core relative to the clastic shoreface facies. Both Runkel et al. (1998) and Saltzman et al. (2004) defined an interval of maximum regression near the top of the *Dunderbergia* zone in a thick limestone/dolostone package as opposed to a single sequence boundary (Fig. 3). The Sauk III transgression occurred throughout the rest of the *Elvinia* Zone. Successions deposited in the Hollandale Embayment therefore represent a wide range of depositional environments and include non-fossiliferous fluvial

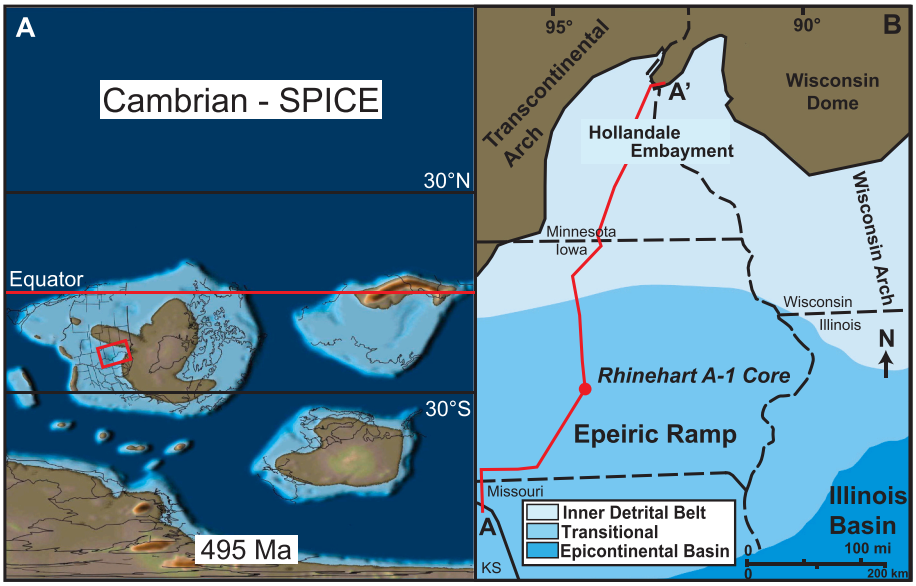

Fig. 1. A) Late Cambrian paleogeography (Scotese, 2014). The red box outlines the area shown in Panel B. B) Reconstruction of the Upper Mississippi Valley region during the Cambrian. The red line A to A' defines the cross section shown in Fig. 2. Red dot indicates the position of the Rhinehart A-1 core (Runkel et al., 1998). (For interpretation of the references to colour in this figure legend, the reader is referred to the web version of this article.)

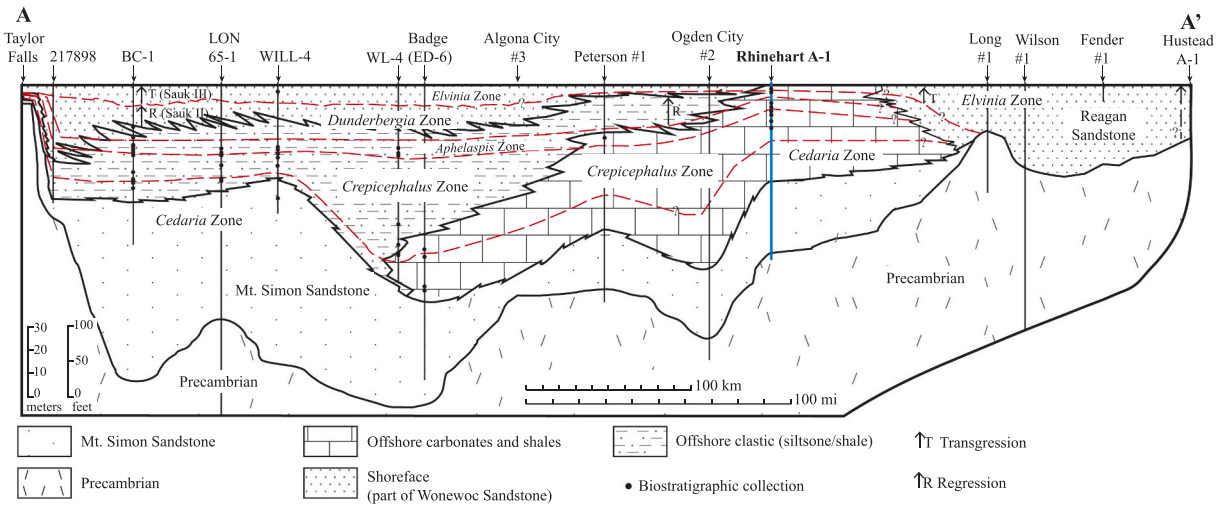

Fig. 2. A roughly south (A) to north (A') cross section depicting the facies and biostratigraphy of the Hollandale Embayment (after Runkel et al., 1998). Location of the Rhinehart A-1 core shown in blue.

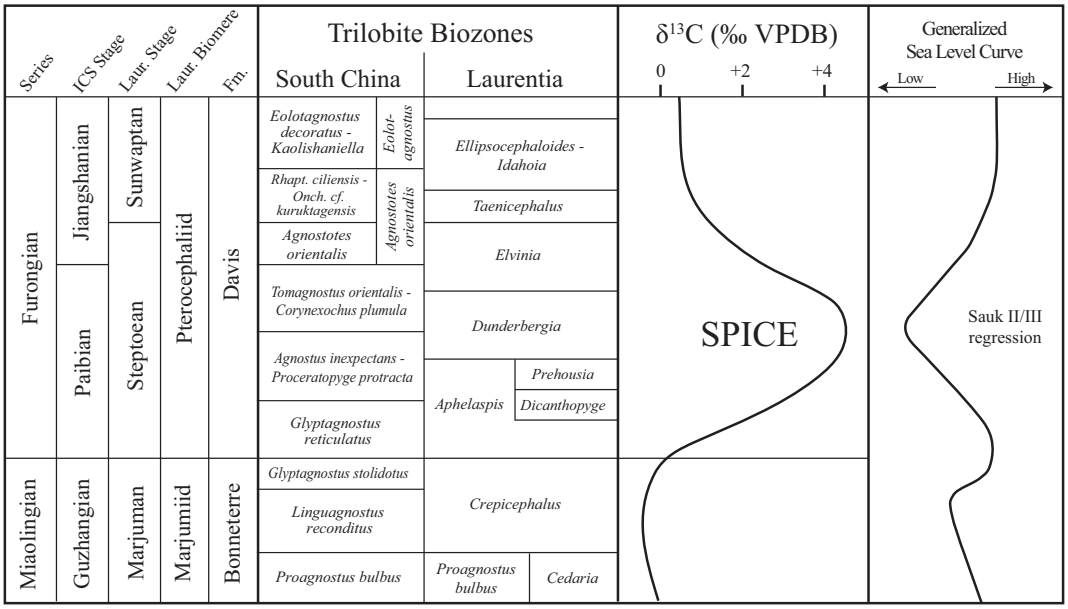

Fig. 3. Maolingian and Furongian trilobite zones and carbon isotope chemostratigraphy of Laurentia and South China with a generalized sea level curve after Zhang et al. (2023). The onset of the SPICE event corresponds to the Crepicephalus-Aphelaspis boundary, the Marjumiid-Pterocephaliid biomere boundary, the base of the North America Steptoean Stage, and the base of the global Paibian Stage, which is defined in South China and is coincident with the First Appearance Datum (FAD) of the trilobite Glyptagnostus reticulatus (Peng et al., 2020).

and eolian deposits, shoreface deposits (cross-bedded sandstones), offshore siliciclastics (very fine sandstones to shales), shallow carbonates, and offshore carbonates and shales (Fig. 2).

The FAD of *Glyptagnostus reticulatus,* a cosmopolitan agnostoid, marks the Global Stratotype Boundary and Section Point (GSSP) for the base of the Paibian Stage and is thus used for global correlation of these strata (Fig. 3). In Laurentia, *G. reticulatus* appears within the *Aphelaspis* Zone, which demarcates the base Steptoean North American Regional Stage and the corresponding Pterocephaliid Biomere (Peng et al., 2020). Therefore, the *Crepicephalus-Aphelaspis* boundary defines the Marjuman-Steptoean North American Regional Stage and Marjumiid-Pterocephaliid biomere boundaries. The onset of the SPICE is contemporaneous with this first appearance of *G. reticulatus* and therefore corresponds to the base Steptoean Stage and Pterocephaliid Biomere (Fig. 3; Saltzman et al., 2000; Peng et al., 2020).

4. Methods

For this study, we obtained 321 samples for carbonate carbon and nitrogen isotope analysis at variable spacing (1-in. [2.54 cm] to 6-in. [15.24 cm] between samples). The samples were most closely spaced immediately prior to the rising limb of the positive $\delta^{13}C_{carb}$ excursion and farthest apart following the peak of the $\delta^{13}C_{carb}$ excursion. Approximately 2 g of powder were generated for each sample by using a drill press with a tungsten carbide drill bit. Roughly 100 mg of powder were separated for $\delta^{13}C_{carb}$ analyses, and 1 g was split for $\delta^{15}N_{bulk}$. We followed the procedure outlined in Hartke et al. (2021) for removal of the carbonate carbon for nitrogen isotope analysis and carried out the decarbonatization process by using 0.5 M HCl. A total of 80 mL of acid was delivered to each sample in 50 mL centrifuge tubes over a series of four rounds with 20 mL per round. After each round, we centrifuged the tubes and decanted the supernatant. To ensure the rinsing of HCl from

each sample, a similar process was repeated following the acid washes with three rounds of deionized water for a total of 60 mL per sample. The samples were then dried in an oven at 40 °C for 3 to 4 days before being homogenized with an agate mortar and pestle, which were cleaned with acetone between each sample. All sample analyses were carried out at the Keck Paleoenvironmental and Environmental Stable Isotope Laboratory at the University of Kansas and all data are available online (Appendix A, Table A1).

4.1. Carbonate carbon

Carbonate powders were reacted via a KIEL Device connected to a ThermoFinnigan MAT 253 isotope ratio mass spectrometer through reaction with 100% phosphoric acid at a density > 1.9 (Wachter and Hayes, 1985). $\delta^{13}C_{carb}$ and $\delta^{18}O_{carb}$ values were calibrated to the VPDB scale using primary standards NBS-18 ($\delta^{13}C_{carb} = -5.01‰$; $\delta^{18}O_{carb} = -23.20‰$) and NBS-19 ($\delta^{13}C_{carb} = 1.95‰$; $\delta^{18}O_{carb} = -2.20‰$), and daily performance of the machine was monitored using laboratory established (secondary) standards SIGMA CALCITE ($\delta^{13}C_{carb} = -18.71‰$; $\delta^{18}O_{carb} = -20.92‰$), TSF-1 ($\delta^{13}C_{carb} = 1.95‰$; $\delta^{18}O_{carb} = -2.20‰$), and 88b Dolomite ($\delta^{13}C_{carb} = 2.06‰$; $\delta^{18}O_{carb} = -6.02‰$), which were analyzed at the beginning, middle, and end of each 40-sample queue. Analytical runs were stopped if the second standard $\delta^{18}O_{carb}$ value (always NBS-18) was >0.17‰ off the standard value, which is the known uncertainty of NBS-18. Carbon and oxygen isotope values derived from carbonates are calibrated using both NBS-18 and NBS-19 due to the known variability when sampling microgram quantities of NBS-19, which is granular and typically fine sand to coarse silt size. The precision of both carbon and oxygen was better than 0.10‰ for all samples analyzed on the basis of repeated measurements of calibration standards, check standards, and sample replicates.

4.2. Nitrogen

Nitrogen isotope samples were weighed and then wrapped in a 5 × 9 mm pressed tin capsule before loading into a Costech Zero Blank Autosampler. From that point forward, the samples and resulting gases were under continuous flow from an Ultrapure Helium gas stream. Sample combustion was carried out with an aliquot of oxygen in a Costech Instruments ECS 4010 Elemental Combustion System. The temperature of the combustion furnace was maintained at 980 °C; however, the ultimate combustion temperature was between 1700 °C and 1800 °C due to the addition of oxygen and tin. Excess oxygen and nitrous compounds were reduced in a reduction furnace maintained at 600 °C. Water was removed with a magnesium perchlorate trap, and the CO_2 and N_2 gases were separated in a GC Column at 50 °C. The separated N_2 gas was interfaced with a ThermoFinnigan MAT 253 isotope ratio mass spectrometer via a ThermoFinnigan Conflo III Device. Samples were analyzed with a suite of primary and secondary stable isotope standards including USGS-25 ($\delta^{15}N = -30.41‰$), USGS-26 ($\delta^{15}N = 53.75‰$), and IAEA-600 ($\delta^{15}N = 1.0‰$). The precision for nitrogen isotope analysis was better than 0.20‰ for all analyses on the basis of repeated measurements of calibration standards, check standards, and sample replicates. Total nitrogen was determined by establishing a linear relationship between peak area of mass 28 (N_2) as measured with the isotope ratio mass spectrometer and nitrogen content. During each analysis several standards of known nitrogen content were measured resulting in a linear regression ($R^2 > 0.99$) used to calculate sample nitrogen content from sample mass 28 areas. The total nitrogen content of each sample was then calculated against the original sample weight of each sample prior to decarbonatization to provide N%.

5. Results

5.1. Carbonate carbon

The Bonneterre Formation at the base of our sampling interval contains $\delta^{13}C_{carb}$ values of +0.80‰ that slowly climb to about +1‰ near the topmost carbonates in the formation (Fig. 4). However, at 2869 ft, values begin rapidly oscillating between +1‰ and + 2‰ in the overlying calcareous shales until 2865.17 ft, which marks the Bonneterre-Davis Formation contact and the approximate onset of the rising limb of the positive $\delta^{13}C_{carb}$ excursion. This brief interval is distinguished by the presence of hematite-, limonite-, and glauconite-rich calcareous shales. Carbonate carbon isotope values then more quickly rise throughout the lower part of the Davis Formation until reaching a maximum value of +3.94‰ at 2845.67 ft. The magnitude of the SPICE $\delta^{13}C_{carb}$ excursion recorded here (~ +4‰ absolute magnitude and ~ +3‰ total change) agree with the findings of Saltzman et al. (2004) who sampled this interval at lower resolution from this core in their work. Peak $\delta^{13}C_{carb}$ values between +3‰ and + 4‰ are generally limited to the most carbonate-dominated intervals of strata and $\delta^{13}C_{carb}$ slowly descend back to a pre-excursion baseline below +1.0‰ during the early stages of the Sauk III transgression.

5.2. Nitrogen

$\delta^{15}N_{bulk}$ values in the lower portion of our sampled interval of the Bonneterre Formation are initially variable, ranging from +2‰ to +8‰ and remain between +4‰ to +8‰ approaching the Bonneterre-Davis boundary (Fig. 4). The beginning of a prominent, transient negative shift in $\delta^{15}N_{bulk}$ is roughly coincident with the contact where $\delta^{15}N_{bulk}$ values rapidly decline to just below 0‰ over a ~ 2 ft. (0.61 m) interval. This negative $\delta^{15}N_{bulk}$ excursion coincides with the earliest interval of the onset of the rising limb of the positive $\delta^{13}C_{carb}$ excursion in the base of the Davis Formation. After reaching minimum values, the $\delta^{15}N_{bulk}$ signature recovers to a short interval of a comparatively steady values of ~ +7‰ before continuing up-section generally varying between +4‰ and + 8‰.

6. Discussion

The results presented here show a clear temporal relationship between a pronounced negative excursion in $\delta^{15}N_{bulk}$ and the initiation of the expanding reduced environments that drove enhanced organic carbon burial and the positive $\delta^{13}C_{carb}$ excursion during the onset of the SPICE event. The entire ~6.0‰ negative $\delta^{15}N_{bulk}$ excursion to values below 0.0‰ was short lived and occurred during the interval where $\delta^{13}C_{carb}$ values began to increase from +1.0‰ to +2.0‰ during the initial onset of the positive carbon isotope excursion. $\delta^{15}N_{bulk}$ values recovered up-section back to more typical marine $\delta^{15}N$ values of +4.0‰ to +8.0‰ for the remainder of the SPICE as well as the post-SPICE interval (Fig. 4).

Here, we define a pre-SPICE interval along with two phases associated with the onset of the SPICE event. Phase 0 is shown as the blue interval in Fig. 4 and represents the approximate pre-excursion baseline $\delta^{13}C_{carb}$ values. The beginning of the yellow interval in Fig. 4 signifies Phase 1 of SPICE initiation wherein $\delta^{13}C_{carb}$ values first begin to oscillate. The Phase 1-Phase 2 boundary corresponds with the Bonneterre-Davis Formation boundary and marks the termination of the rapidly varying $\delta^{13}C_{carb}$ values. Phase 2 (red box in Fig. 4) encapsulates the onset of steadily rising $\delta^{13}C_{carb}$ values, the negative $\delta^{15}N_{bulk}$ excursion, and the return to mean ocean $\delta^{15}N_{bulk}$ values. This is the first time that a negative perturbation to the marine nitrogen cycle has been identified during the initiation of the SPICE event (see Hammer and Svensen, 2017) and is the first observed local record of what may have been a fundamental reorganization of biogeochemical nutrient cycling as the cascade of changes that triggered the SPICE event played out. A similar

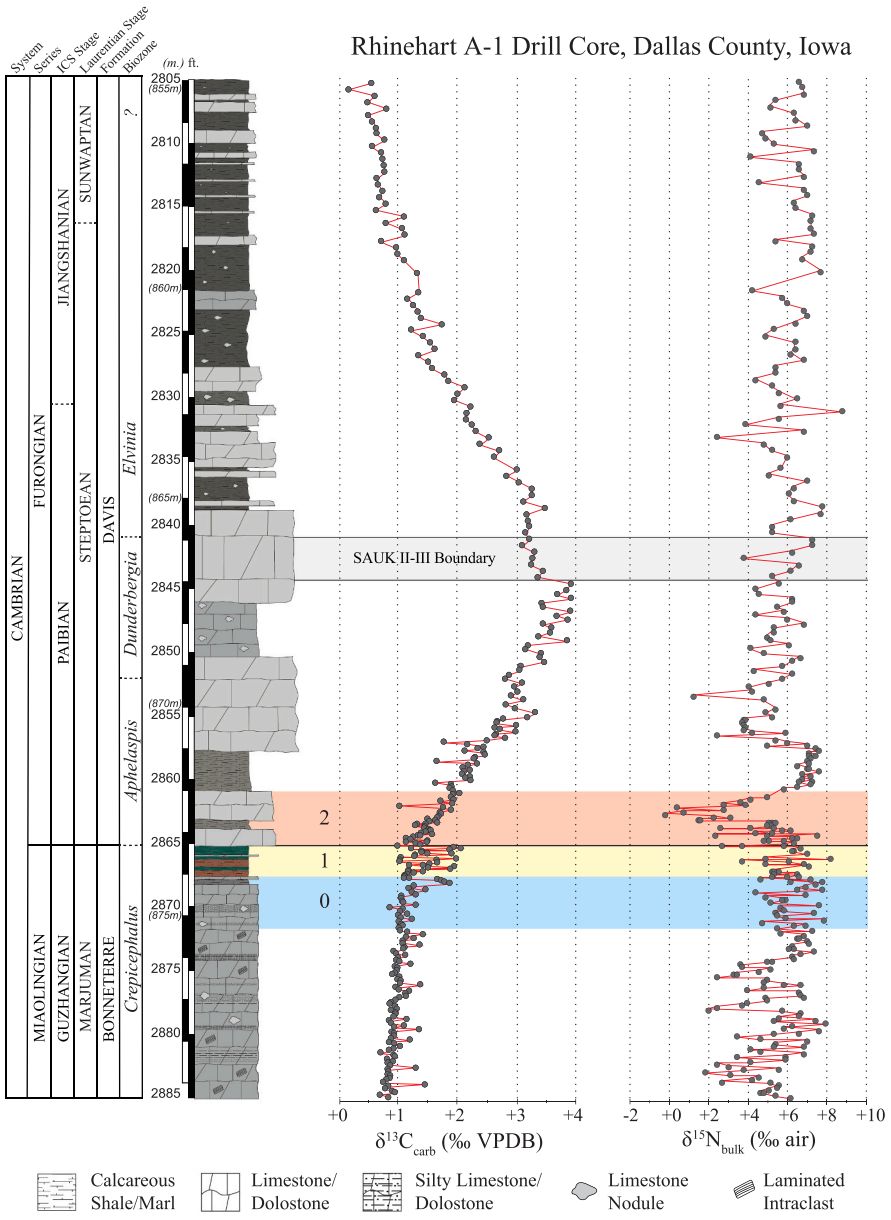

Fig. 4. $\delta^{13}C_{carb}$ and $\delta^{15}N_{bulk}$ record of the SPICE event in the Rhinehart A-1 core. The blue, yellow, and red intervals highlight the pre-SPICE interval, Phase 1 of initiation, and Phase 2 of initiation of the SPICE event, respectively. See discussion for further definition of each phase. The initial impacts in the carbon cycle and sedimentary abundance of hematite and glauconite first appear in Phase 1, whereas the negative $\delta^{15}N_{bulk}$ excursion and initiation of the rising limb of the positive $\delta^{13}C_{carb}$ excursion take place during Phase 2. (For interpretation of the references to colour in this figure legend, the reader is referred to the web version of this article.)

relationship between expanding reduced environments, global carbon cycle perturbations, and marine nutrient cycling has been well documented during the Cretaceous Oceanic Anoxic Event 2 (OAE2; e.g., Mort et al., 2007; Junium and Arthur, 2007; Monteiro et al., 2012; Ruvalcaba Baroni et al., 2015; Zhang et al., 2019), which provides important insight into the initiation of the SPICE event.

6.1. Preservation of the marine nitrogen isotope record

The sedimentary record of $\delta^{15}N$ can provide a robust proxy for changes in nitrogen cycling and bioavailable N availability in the overlying water column (Kuypers et al., 2004; Junium and Arthur, 2007; Higgins et al., 2012; Liu et al., 2015; Ruvalcaba Baroni et al., 2015; Zhang et al., 2019). However, bulk sedimentary $\delta^{15}N$ values are susceptible to alteration during diagenesis (e.g., Robinson et al., 2012; Ader et al., 2016), and care must be taken to ensure the $\delta^{15}N$ record of a given stratigraphic section faithfully records changes in the marine N system. A series of cross plots of Total Nitrogen (TN), Total Organic Carbon (TOC), $\delta^{15}N_{bulk}$, and percent carbonate are provided (Fig. 5) to evaluate the potential influence of diagenesis on the nitrogen isotope record from the Rhinehart A-1 core.

The $\delta^{15}N_{bulk}$ values of organic-poor sediments, such as those included in this study, can be more easily impacted by the amount of inorganic nitrogen incorporated into the sediment, and a positive TN intercept on the plot of TN vs. TOC implies such an alteration of the primary $\delta^{15}N$ signal may have occurred (e.g., Calvert, 2004; Kienast et al., 2005). Whereas there are two clear populations of samples in our data (Fig. 5A), one of which carries a linear relationship with $R^2 = 0.7062$, both populations have a negligible intercept of the TN axis (−0.0006 and + 0.0013). This relationship suggests that the majority of the bulk N sampled in this study likely comes from organic matter and that the potential impact of inorganic N on the $\delta^{15}N_{bulk}$ record in this

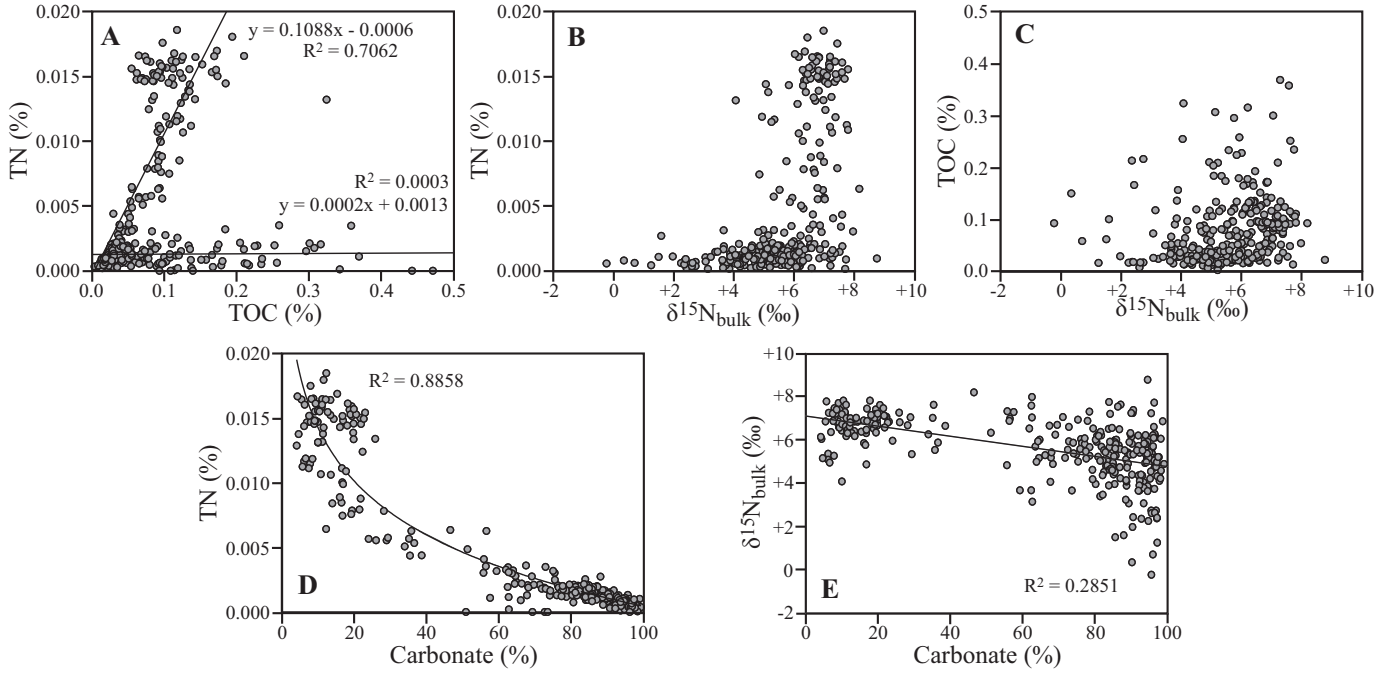

Fig. 5. Total Nitrogen (TN), Total Organic Carbon (TOC), Carbonate %, and $\delta^{15}N_{bulk}$ cross plots of the data from the Rhinehart A-1 core. A) TN vs. TOC show negligible intercepts on the TN axis, which is consistent with the primary source of sampled N coming from organic matter. B) Neither TN, nor C) TOC show any significant correlation with $\delta^{15}N_{bulk}$ and do not appear to be responsible for the negative $\delta^{15}N_{bulk}$ excursion. D) TN show an inverse logarithmic correlation to carbonate %. E) The two end-member lithologies of calcareous shale (marl) and limestone show little correlation with $\delta^{15}N_{bulk}$ record and do not appear to be responsible for the negative $\delta^{15}N_{bulk}$ excursion.

study should be minimal.

The comparisons of TN vs. $\delta^{15}N_{bulk}$ and TOC vs. $\delta^{15}N_{bulk}$ (Figs. 5B and C) show little-to-no correlation between either TN or TOC with $\delta^{15}N_{bulk}$, which further supports the reliability of the N-isotope data from the Rhinehart A-1 core. The overwhelming majority of $\delta^{15}N_{bulk}$ values are between +4.0‰ and + 8.0‰ for both the low- and high-TN populations in this study, and the negative $\delta^{15}N_{bulk}$ excursion that is the focus of this investigation takes place entirely within the low-TN group. The TN content is well correlated ($R^2 = 0.8858$) to carbonate percent in each sample and shows a clear inverse logarithmic relationship (Fig. 5D); however, this relationship between TN and carbonate percent is not a significant influence on $\delta^{15}N_{bulk}$ (Fig. 5E). The relationship between $\delta^{15}N_{bulk}$ values and lithology (Fig. 5E) highlights the two populations where the carbonate-rich strata are primarily clustered between +4.0‰ and + 6.0‰, and the marly and more clay-rich strata are primarily clustered between +6.0‰ and + 8.0‰. However, the most significant feature of the data presented here (Figs. 4 and 5) is that the negative $\delta^{15}N_{bulk}$ excursion takes place exclusively in a single lithology (limestone), does not correlate with sea level trends in this interval (i.e., not centered on the Sauk II-III sequence boundary and not an artifact of facies changes), and does not show any clear relationship with TOC or TN in the section. Therefore, we suggest that the $\delta^{15}N_{bulk}$ values in the Rhinehart A-1 core are primarily recording the original isotopic composition of nutrient N incorporated into marine organic matter and that the negative excursion in $\delta^{15}N_{bulk}$ represents at least a local perturbation to the marine nitrogen cycle during the initiation of the SPICE event.

6.2. Carbon cycle perturbations, reducing environments, and the SPICE event

The preferential uptake of ^{12}C during photosynthesis imparts a fractionation of carbon in organic matter, and marine phytoplankton typically carry a $\delta^{13}C$ value (i.e., $^{13}C/^{12}C$) significantly enriched in ^{12}C compared to the isotopic value of CO_2 in the ocean-atmosphere system. Therefore, any partitioning and burial of marine organic carbon will have the effect of preferentially removing ^{12}C from the system and leaving the remaining marine carbon pool with an increased $\delta^{13}C$ value (e.g., Hayes et al., 1999; Falkowski, 2003; Ciais et al., 2013; Cramer and Jarvis, 2020). In fully oxygenated oceans, organic carbon is typically respired and converted back into CO_2, and the complete photosynthesis-respiration loop imparts no net change to the $\delta^{13}C$ value of ocean-atmosphere system. However, in reducing environments (anoxic or euxinic), oxidative respiration is extremely limited, and a significantly higher fraction of organic carbon reaching the sediment-water interface is buried and preserved. This effectively partitions ^{12}C into the lithosphere and generates an increase in the $\delta^{13}C$ value of the residual carbon pool in the ocean-atmosphere system that can ultimately be preserved as a positive $\delta^{13}C$ excursion in the stratigraphic record. These fundamental controls of photosynthesis, redox, and organic carbon burial on the marine $\delta^{13}C$ record help to explain the relationships between times of expanding reducing environments, such as during oceanic anoxic events (OAEs), and positive $\delta^{13}C$ excursions seen throughout the Phanerozoic (e.g., Cramer and Jarvis, 2020).

Variations in marine biogeochemical cycling of redox-sensitive elements, such as S, Mo, U, V, Fe, and Hg, are excellent proxies for secular change in the redox state of ancient oceans. The speciation, abundance, and/or isotopic compositions of these elements have been employed to investigate changes in oceanic redox during the SPICE event, and over the past decade, a clear consensus has developed that the SPICE event is very likely related to an expansion of reducing environments during an OAE (Saltzman et al., 2011; Gill et al., 2011; Dahl et al., 2014; Pruss et al., 2019; LeRoy and Gill, 2019; LeRoy et al., 2021; Gill et al., 2021; Zhang et al., 2023; Zhao et al., 2023). This transition to increased anoxia/euxinia served to increase organic carbon burial and drive the positive $\delta^{13}C$ excursion during the SPICE event.

Unfortunately, the initial trigger for the expansion of reducing environments, and ultimately the SPICE event itself, remains enigmatic (e.g., Rooney et al., 2022; Zhang et al., 2023; Zhao et al., 2023). A decrease in marine oxygenation can be driven by either increased oxygen demand

from sinking organic matter produced in the photic zone (e.g., Mort et al., 2007; Monteiro et al., 2012; Naafs et al., 2019) or decreased oxygen supply from an oceanographic reduction in oxygenated surface waters reaching the sediment-water interface (e.g., Wignall, 1991; Pohl et al., 2022). Both of these factors (productivity-driven anoxia vs. oceanographically-driven anoxia) have been invoked to explain Phanerozoic biogeochemical perturbations. In addition, estimates of atmospheric O_2 concentrations during the Cambrian suggest that they may have been significantly <50% of present atmospheric levels (Dahl et al., 2017; Lenton et al., 2018; Schachat et al., 2018; Mills et al., 2023), which would have necessarily decreased marine oxygenation compared to the modern ocean and perhaps made the Cambrian oceans more susceptible to deoxygenating factors. Deciphering the dominant control responsible for the expansion of reducing environments is challenging (productivity, oceanography, or both), and a single core from a single locality, such as presented here, certainly cannot provide a global answer to this question. However, a detailed examination of nutrient cycling and marine redox dynamics on a local scale provides a critical step towards enhancing the current understanding of the temporal and spatial nature of global ocean redox conditions during the Cambrian SPICE. Further, the relationships shown here between nitrogen cycling, deoxygenation of marine environments, and the onset of a global carbon cycle perturbation during the SPICE event are almost identical to those seen during the onset of the Cretaceous OAE2, which serves as a critical comparison to evaluate the biogeochemical signals preserved in the Rhinehart A-1 core.

6.3. *Primary productivity, nitrogen cycling, and the onset of the SPICE event*

The expansion of reducing environments during the initial onset of the SPICE event has been well-documented (e.g., Zhang et al., 2023; Zhao et al., 2023) and would hold significant implications for biogeochemical nutrient cycling in the marine realm. The resulting cascade of events are well-preserved in the Rhinehart A-1 core (Figs. 4 and 6) and show striking similarities with other major biogeochemical events, such as the Cretaceous OAE2 (Mort et al., 2007; Monteiro et al., 2012; Ruvalcaba Baroni et al., 2015; Zhang et al., 2019). As reducing environments expanded into previously oxygenated settings, phosphorous bound to iron oxy-hydroxides and/or organic matter would begin to be remobilized (Van Cappellen and Ingall, 1994; Saltzman, 2005). This would have liberated both Fe as well as P back into the water column, stimulating primary productivity and initiating a decrease in N:P in surface waters (Fig. 6B). This "Phase 1" of initiation of the SPICE event (yellow area in Fig. 4; "Phase 1" Fig. 6B) contains the first evidence of the start of a carbon cycle perturbation as well as significant sedimentary Fe enrichment in the Rhinehart A-1 core present as glauconite, hematite, and limonite grains (Fig. 4).

At the same time that P delivery was increasing, N availability was decreasing due to increased removal of nutrient N through enhanced primary productivity in surface waters and enhanced denitrification/anammox/DNRA in underlying oxygen minimum zones. This imbalance would have progressed until the N:P ratio was sufficiently low to favor diazotrophy and initiate enhanced N-fixation to compensate ("Phase 2" Fig. 6C). The incorporation of this "new" fixed N into primary production drove the negative $\delta^{15}N_{bulk}$ excursion, which was the sedimentary record of this discrete interval of N stress in the Laurentian mid-continent. If the oxygen minimum zone impinged upon the photic zone, direct incorporation of NH_4^+ could have additionally contributed to the negative $\delta^{15}N_{bulk}$ excursion. This severe imbalance in N:P and interval of acute N stress was limited to the initial onset of the SPICE event. $\delta^{15}N_{bulk}$ values quickly recovered to more "normal" marine values during the remainder of the rising limb of the positive $\delta^{13}C_{carb}$ excursion and remained there throughout the rest of the sampled interval of the core.

That the negative $\delta^{15}N_{bulk}$ excursion is restricted to the initial onset of the SPICE event and does not persist even through the entire rising limb of the positive $\delta^{13}C_{carb}$ excursion suggests that anoxia and the removal of nutrient N through denitrification/anammox/DNRA alone was not likely to have been the only, or even primary, driver of the N:P imbalance that favored diazotrophy. The liberation of P, and particularly Fe, during the initial expansion of reducing environments may have

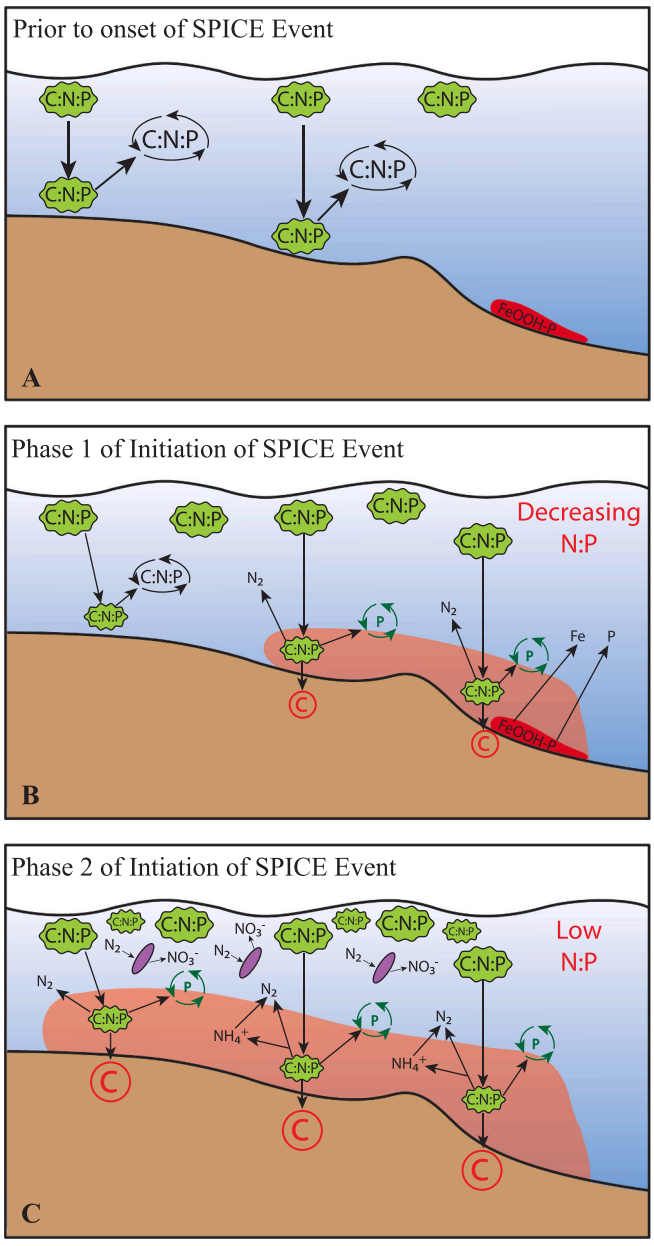

Fig. 6. Three-step schematic model of the onset of the SPICE event as recorded in the Rhinehart A-1 core. A) Shelf environment prior to the onset of the $\delta^{13}C_{carb}$ excursion. Regular nutrient cycling of carbon, nitrogen, and phosphorus occur throughout the water column. Green circles represent primary producers/biomass, and the red area represents a small reducing environment where P adsorbs onto Fe oxy-hydroxides. B) Phase 1 of initiation of the SPICE event. Expansion of reducing environments (pink area), potentially from enhanced continental weathering (Rooney et al., 2022), remobilizes additional P and Fe. Denitrification/anammox/DNRA and enhanced primary productivity begin to deplete the marine fixed N inventory and lower the N:P ratio of surface waters. C) Further expansion of reducing environments and primary production lower the N:P ratio to the point where consortia of diazotrophic nitrogen fixation (diazotrophs shown as purple ellipses) and nitrification begin to produce a larger percentage of bioavailable fixed N, which creates the negative $\delta^{15}N_{bulk}$ excursion. (For interpretation of the references to colour in this figure legend, the reader is referred to the web version of this article.)

provided the required push into extreme N stress where the addition of these two critically bio-limiting nutrients precipitated a rapid increase in primary productivity that the existing marine fixed N inventory could not accommodate. However, as reduction progressed and anoxia transitioned into euxinia, Fe would have been increasingly scavenged by H_2S to form pyrite (Saltzman et al., 2011; Zhang et al., 2023; Zhao et al., 2023), providing a negative feedback to this critical biogeochemical cycle.

Whereas the biogeochemical feedbacks within the marine system discussed above can help to explain the data recovered from the Rhinehart A-1 core, they still do not address the initial trigger that created the SPICE event. The scenario presented here (Fig. 6) of enhanced nutrient delivery leading to increased primary productivity, further expanding deoxygenation, enhanced organic carbon burial, and ultimately N-stress and a negative excursion in $\delta^{15}N$ at the start of a positive $\delta^{13}C$ excursion has been well documented from Cretaceous strata during OAE2 (Mort et al., 2007; Monteiro et al., 2012; Ruvalcaba Baroni et al., 2015; Zhang et al., 2019), and our data from the SPICE event in the Laurentian epicontinental interior are strikingly similar.

Zhang et al. (2019) produced $\delta^{15}N_{bulk}$ data from the Gongzha section in present-day southern Tibet, formerly located in the eastern Tethys during the Cretaceous. The lowest $\delta^{15}N_{bulk}$ values coincide with the onset of the positive $\delta^{13}C_{carb}$ excursion (Fig. 7), which is consistent with N isotopic data from equivalent sections in other paleogeographic regions (Junium and Arthur, 2007; Higgins et al., 2012; Ruvalcaba Baroni et al., 2015). They attribute the influx of isotopically light N to the expansion of marine anoxia; an expansion of anoxia would have decreased the bioavailable N reservoir via increased denitrification and anammox, subsequently triggering enhanced N_2 fixation by diazotrophs as they gained a competitive advantage in a low N:P environment (Zhang et al., 2019). We propose a similar sequence of events here to explain the negative $\delta^{15}N_{bulk}$ excursion at the onset of the SPICE event.

During the Cretaceous, the initial trigger of OAE2 was the emplacement of a Large Igneous Province (LIP) and the concomitant perturbations to CO_2, weathering, and nutrient delivery to the oceans that followed (Mort et al., 2007; Turgeon and Creaser, 2008; Monteiro et al., 2012; DuVivier et al., 2014; Jenkyns et al., 2017). Only recently have similar hypotheses begun to be tested for the potential trigger of the SPICE event. Re, Os, and Nd isotope data from the Alum Shale Formation (Sweden) demonstrated that a LIP, or similar emplacement of mafic volcanism, was not responsible for the initiation of the SPICE event (Rooney et al., 2022) but that there appears to have been a marked increase in continental weathering during the initial onset of the SPICE. Specifically, $^{187}Os/^{188}Os$ values rise rapidly during the initiation of the SPICE event, which is the opposite of what would be expected from LIP emplacement (e.g., Turgeon and Creaser, 2008; DuVivier et al., 2014) but is consistent with increased delivery of radiogenic Os values to the global ocean via enhanced continental weathering (Rooney et al., 2022). This positive peak in $^{187}Os/^{188}Os$ values significantly preceded the Sauk II-III sequence boundary (and maximum regression) and aligns more closely with the negative $\delta^{15}N_{bulk}$ excursion reported here, suggesting that changes in eustatic sea level alone were likely not the only mechanism responsible for enhanced continental weathering. Even though the resolution of the $^{187}Os/^{188}Os$ data do not allow a definitive high-resolution correlation to our present study, it is clear that LIP emplacement was not likely to have been responsible and that there was

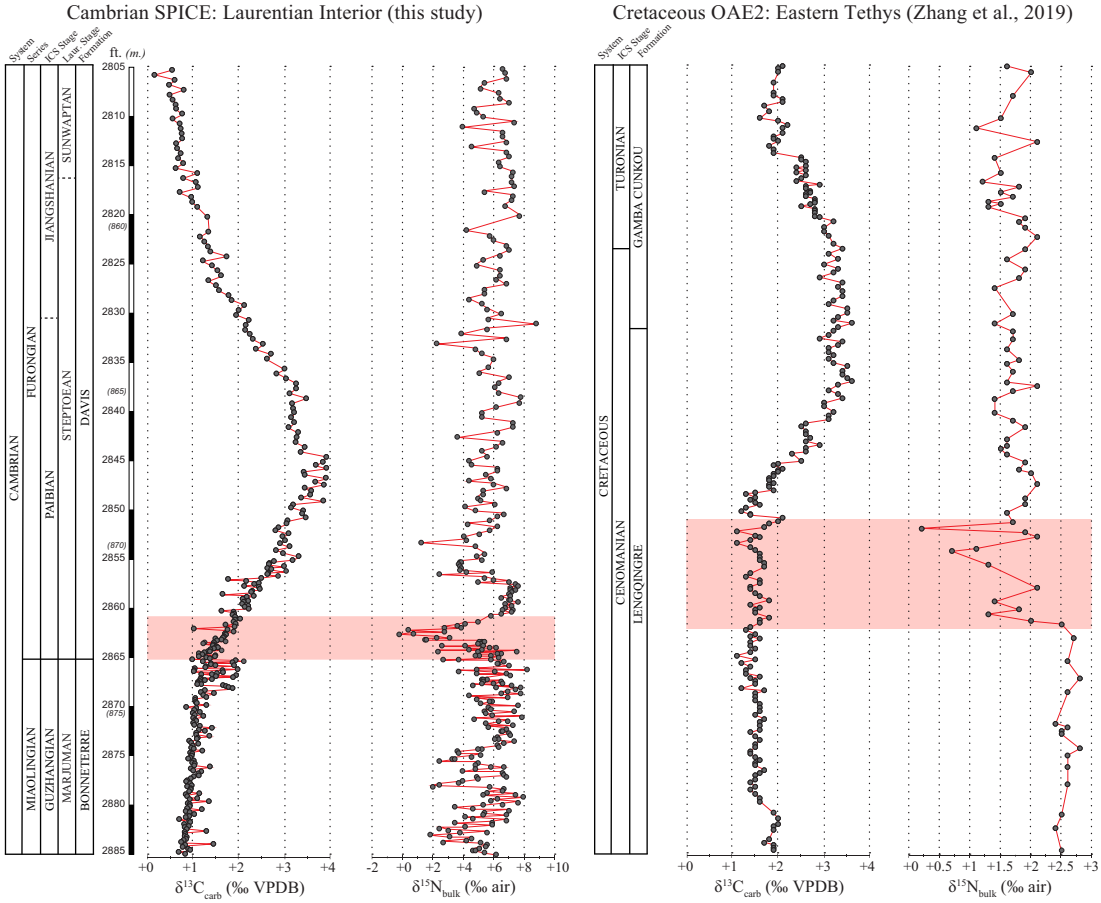

Fig. 7. A comparison of the $\delta^{13}C_{carb}$ and $\delta^{15}N_{bulk}$ records of the Cambrian SPICE event preserved in the Laurentian midcontinent and Cretaceous OAE2 preserved in an eastern Tethys section. OAE2 data are from Zhang et al. (2019). A negative excursion in $\delta^{15}N_{bulk}$ (shown as red interval) is present at the initiations of both the SPICE event and OAE2 positive $\delta^{13}C_{carb}$ excursion.

a brief interval of enhanced continental weathering during the initiation of the positive $\delta^{13}C$ excursion. This enhanced delivery of continentally-derived nutrients to the ocean could then have been an additional critical force that ultimately triggered the SPICE event.

7. Conclusions

The paired high-resolution carbon and nitrogen isotope data from the Rhinehart A-1 core show a pronounced negative $\delta^{15}N_{bulk}$ excursion coincident with the initiation of the rising limb of the positive $\delta^{13}C_{carb}$ excursion, both of which are consistent with enhanced primary productivity and a disruption of the marine N cycle during the onset of the SPICE event. The comparison of these new data to recent S, U, Mo, and Os isotope data from the SPICE event (Rooney et al., 2022; Zhang et al., 2023; Zhao et al., 2023) demonstrate the importance of High-Resolution Integrated Event Stratigraphy (HiRES, Cramer et al., 2015) to investigations of the cascade of short-lived events that make up global biogeochemical perturbations. Our new data provide evidence of significant changes in local primary productivity and biogeochemical nutrient cycling during the initiation of Paibian global change that help to shed new light on the possible trigger(s) of the SPICE event and provide comparisons with other Phanerozoic biogeochemical events.

Reduced environments began to expand during the latest Guzhangian (Saltzman et al., 2011; Gill et al., 2011; LeRoy and Gill, 2019; LeRoy et al., 2021; Zhang et al., 2023; Zhao et al., 2023), which remobilized both Fe and P that had been previously bound to iron oxyhydroxides (Van Cappellen and Ingall, 1994; Saltzman, 2005). Recent Os isotope data (Rooney et al., 2022) suggest there was a concurrent increase in terrestrial weathering that would have provided additional riverine delivery of these bio-limiting nutrients, and together, these changes would have significantly enhanced primary production through eutrophication. This enhanced delivery of P, combined with the negative impacts of anoxia on the marine fixed N inventory (Falkowski et al., 1998; Tyrrell, 1999; Lenton and Watson, 2000), lowered the N:P ratio to the point that diazotrophic N fixation (and/or direct uptake of NH_4^+ if the OMZ expanded into the photic zone) became a major contributor to the bioavailable fixed N pool. The result was a significant negative $\delta^{15}N_{bulk}$ excursion to ~0.0‰ that did not persist throughout the entire positive $\delta^{13}C_{carb}$ excursion but was instead limited to a short-lived interval during the initial onset of the SPICE event. $\delta^{15}N_{bulk}$ excursion values recovered to pre-event values during the remainder of the rising limb of the $\delta^{13}C_{carb}$ excursion and stayed there throughout the post-SPICE interval, thus suggesting the imbalance in N:P, the pulse of enhanced primary productivity, and the perturbation to the marine N cycle was limited to initial onset of the SPICE event.

The relationship seen here between a negative $\delta^{15}N_{bulk}$ excursion coinciding with the onset of a positive $\delta^{13}C_{carb}$ excursion has been well documented during the Cretaceous OAE2 (e.g., Ruvalcaba Baroni et al., 2015; Zhang et al., 2019), where additional data support the role of P delivery as a critical driver of that event (e.g., Mort et al., 2007; Monteiro et al., 2012). Recent investigations of other Paleozoic OAEs have begun to illustrate similar changes in nutrient cycling, primary productivity, and the onset of organic carbon burial from the Ireviken (Silurian) and Hangenberg (Devonian-Carboniferous Boundary) events as well (Pisarzowska et al., 2020; Hartke et al., 2021; Heath et al., 2021; Stolfus et al., 2023) and may illustrate that there are a set of common events that took place during many OAEs. Whereas the LIP trigger proposed for OAE2 does not appear to have been the case for the SPICE event (Rooney et al., 2022), enhanced delivery of continentally-derived nutrients is beginning to appear to play a common role in many of these events (e.g., Pisarzowska et al., 2020; Sproson et al., 2022) as eutrophication and enhanced primary productivity took place during the initiation of these major biogeochemical events.

CRediT authorship contribution statement

Gwen L. Barnes: Writing – original draft, Conceptualization. **Bradley D. Cramer:** Writing – review & editing, Supervision, Funding acquisition, Conceptualization.

Declaration of competing interest

The authors declare that they have no known competing financial interests or personal relationships that could have appeared to influence the work reported in this paper.

Data availability

The data file is available in Appendix A.

Acknowledgments

We thank editor Maoyan Zhu and co-editor Lynn Soreghan for handling this manuscript. We also thank L. Soreghan, B. Gill, and an anonymous reviewer for constructive comments that strengthened this paper. This research was partially supported by grants from the U.S. National Science Foundation to B.D. Cramer (CAREER-1455030 and EPSCOR-2119551) and was conducted as an undergraduate senior thesis project by G.L. Barnes at the University of Iowa, Department of Earth and Environmental Sciences. We thank B. Barnett at the University of Kansas, Keck Paleoenvironmental and Environmental Stable Isotope Laboratory (KPESIL) for producing the carbon and nitrogen isotope analyses.

Appendix A. Supplementary data

Supplementary data to this article can be found online at https://doi.org/10.1016/j.gloplacha.2024.104365.

References

Ader, M., Thomazo, C., Sansjofre, P., Busigny, V., Papineau, D., Laffont, R., Cartigny, P., Halverson, G.P., 2016. Interpretation of the nitrogen isotopic composition of Precambrian sedimentary rocks: assumptions and perspectives. Chem. Geol. 429, 93–110. https://doi.org/10.1016/j.chemgeo.2016.02.010.

Ahlberg, P., Lundberg, F., Erlström, M., Calner, M., Lindskog, A., Dalhqvist, P., Joachimski, M.M., 2019. Integrated Cambrian biostratigraphy and carbon isotope chemostratigraphy of the Grönhögen-2015 drill core, Öland, Sweden. Geol. Mag. 156, 935–949. https://doi.org/10.1017/S0016756818000298.

Bachan, A., Lau, K.V., Saltzman, M.R., Thomas, E.T., Kump, L.R., Payne, J.L., 2017. A model for the decrease in amplitude of carbon isotope excursions across the Phanerozoic. Am. J. Sci. 317, 641–676. https://doi.org/10.2475/06.2017.01.

Calvert, S.E., 2004. Beware intercepts: interpreting compositional ratios in multi-component sediments and sedimentary rocks. Org. Geochem. 35, 981–987. https://doi.org/10.1016/j.orggeochem.2004.03.001.

Ciais, P., Sabine, C., Bala, G., Bopp, L., Brovkin, V., Canadell, J., Chhabra, A., DeFries, R., Galloway, J., Heimann, M., Jones, C., Le Qu'er'e, C., Myneni, R.B., Piao, S., Thornton, P., 2013. Carbon and other biogeochemical cycles. In: Stocker, T.F., Qin, D., Plattner, G.K., Tignor, M., Allen, S.K., Boschung, J., Midgley, P.M. (Eds.), Climate Change 2013: The Physical Science Basis. Contribution of Working Group I to the Fifth Assessment Report of the Intergovernmental Panel on Climate Change. Cambridge University Press, Cambridge, United Kingdom, pp. 465–570.

Cothren, H.R., Farrell, T.P., Sundberg, F.A., Dehler, C.M., Schmitz, M.D., 2022. Novel age constraints for the onset of the Steptoean positive Isotopic Carbon Excursion (SPICE) and the late Cambrian time scale using high-precision U-Pb detrital zircon ages. Geology 50, 1415–1420. https://doi.org/10.1130/G50434.1.

Cramer, B.D., Jarvis, I., 2020. Chapter 11: Carbon Isotope Stratigraphy. In: Gradstein, F. M., Ogg, J.G., Schmitz, M.D., Ogg, G.M. (Eds.), Geologic Time Scale 2020, vol. 1. Elsevier, Amsterdam, pp. 309–343. https://doi.org/10.1016/B978-0-12-824360-2.00011-5.

Cramer, B.D., Vandenbroucke, T.R.A., Ludvigson, G.A., 2015. High-resolution event stratigraphy (HiRES) and the quantification of stratigraphic uncertainty: Silurian examples of the quest for precision in stratigraphy. Earth Sci. Rev. 141, 136–153. https://doi.org/10.1016/j.earscirev.2014.11.011.

Dahl, T.W., Boyle, R.A., Canfield, D.E., Connelly, J.N., Gill, B.C., Lenton, T.M., Bizzaro, M., 2014. Uranium isotopes distinguish two geochemically distinct stages during the later Cambrian SPICE event. Earth Planet. Sci. Lett. 401, 313–326. https://doi.org/10.1016/j.epsl.2014.05.043.

Dahl, T.W., Connelly, J.N., Kouchinsky, A., Gill, B.C., Manson, S.F., Bizzarro, M., 2017. Reorganization of Earth's biogeochemical cycles briefly oxygenated the oceans 520 Myr ago. Geochem. Perspect. Lett. 210-220, 1724. https://doi.org/10.7185/geochemlet.1724.

DuVivier, A.D.C., Selby, D., Sageman, B.B., Jarvis, I., Gröcke, D.R., Voigt, S., 2014. Marine $^{187}Os/^{188}Os$ isotope stratigraphy reveals the interaction of volcanism and ocean circulation during Oceanic Anoxic Event 2. Earth Planet. Sci. Lett. 389, 23–33. https://doi.org/10.1016/j.epsl.2013.12.024.

Falkowski, P., 2003. Biogeochemistry of primary production in the sea. Treat. Geochem. 8, 185–213. https://doi.org/10.1016/B0-08-043751-6/08129-9.

Falkowski, P.G., Barber, Smetacek, R.T., 1998. Biogeochemical controls and feedbacks on ocean primary production. Science 281, 200–207. https://doi.org/10.1126/science.281.5374.200.

Gill, B.C., Lyons, T.W., Young, S.A., Kump, L.R., Knoll, A.H., Saltzman, M.R., 2011. Geochemical evidence for widespread euxinia in the later Cambrian Ocean. Nature 469, 80–83. https://doi.org/10.1038/nature09700.

Gill, B.C., Dahl, T.W., Hammarlund, E.U., LeRoy, M.A., Gordon, G.W., Canfield, D.E., Anbar, A.D., Lyons, T.W., 2021. Redox dynamics of later Cambrian oceans. Palaeogeogr. Palaeoclimatol. Palaeoecol. 581, 110623 https://doi.org/10.1016/j.palaeo.2021.110623.

Gruber, N., 2004. The Dynamics of the Marine Nitrogen Cycle and its Influence on Atmospheric CO_2 Variations. In: Follows, M., Oguz, T. (Eds.), The Ocean Carbon Cycle and Climate, NATO Science Series (Series IV: Earth and Environmental Sciences), 40. Springer, Dordrecht, pp. 97–148. https://doi.org/10.1007/978-1-4020-2087-2_4.

Gruber, N., Galloway, J.N., 2008. An Earth-system perspective of the global nitrogen cycle. Nature 451, 293–296. https://doi.org/10.1038/nature06592.

Gruber, N., Sarmiento, J.L., 1997. Global patterns of marine nitrogen fixation and denitrification. Glob. Biogeochem. Cycles 11 (2), 235–266. https://doi.org/10.1029/97GB00077.

Hammer, O., Svensen, H.H., 2017. Biostratigraphy and carbon and nitrogen geochemistry of the SPICE event in Cambrian low-grade metamorphic black shale, Southern Norway. Palaeogeogr. Palaeoclimatol. Palaeoecol. 468, 216–227. https://doi.org/10.1016/j.palaeo.2016.12.016.

Haq, B.U., Schutter, S.R., 2008. A chronology of Paleozoic Sea-level changes. Science 322 (5898), 64–68. https://doi.org/10.1126/science.11616.

Hartke, E.R., Cramer, B.D., Calner, M., Melchin, M.J., Barnett, B.A., Oborny, S.C., Bancroft, A.M., 2021. Decoupling $\delta^{13}C_{carb}$ and $\delta^{13}C_{org}$ at the onset of the Ireviken Carbon Isotope Excursion: $\delta^{13}C$ and organic carbon burial (f_{org}) during a Silurian oceanic anoxic event. Glob. Planet. Chang. 196, 103373 https://doi.org/10.1016/j.gloplacha.2020.103373.

Hayes, J.M., Strauss, H., Kaufman, A.J., 1999. The abundance of ^{13}C in marine organic matter and isotopic fractionation in the global biogeochemical cycle of carbon during the past 800 Ma. Chem. Geol. 161, 103–125. https://doi.org/10.1016/S0009-2541(99)00083-2.

Heath, M.N., Cramer, B.D., Stolfus, B.M., Barnes, G.L., Clark, R.J., Day, J.E., Barnett, B. A., Witzke, B.J., Hogancamp, N.J., Tassier-Surine, S.A., 2021. Chemoautotrophy as the driver of decoupled organic and carbonate carbon isotope records at the onset of the Hangenberg (Devonian-Carboniferous Boundary) Oceanic Anoxic Event. Palaeogeogr. Palaeoclimatol. Palaeoecol. 577, 110540 https://doi.org/10.1016/j.palaeo.2021.110540.

Higgins, M.B., Robinson, R.S., Husson, J.M., Pearson, A., 2012. Dominant eukaryotic export production during ocean anoxic events reflects the importance of recycled $NH4^+$. Proc. Natl. Acad. Sci. 109 (7), 2269–2274. https://doi.org/10.1073/pnas.110431310.

Hutchins, D.A., Capone, D.G., 2022. The marine nitrogen cycle: new developments and global change. Nat. Rev. Microbiol. 20, 401–414. https://doi.org/10.1038/s41579-022-00687-z.

Jenkyns, H.C., Dickson, A.J., Ruhl, M., van den Boorn, S.H.J.M., 2017. Basalt-seawater interaction, the Plenus Cold Event, enhanced weathering and geochemical change: Deconstructing Oceanic Anoxic Event 2 (Cenomanian-Turonian, late cretaceous). Sedimentology 64, 16–43. https://doi.org/10.1111/sed.12305.

Junium, C.K., Arthur, M.A., 2007. Nitrogen cycling during the cretaceous, Cenomanian-Turonian Oceanic Anoxic Event II. Geochem. Geophys. Geosyst. 8 (3), Q03002. https://doi.org/10.1029/2006GC001328.

Kienast, M., Higginson, M.J., Mollenhauer, G., Eglinton, T.I., Chen, M.-T., Calvert, S.E., 2005. On the sedimentological origin of down-core variations of bulk sedimentary nitrogen isotope ratios. Paleoceanography 20, PA2009. https://doi.org/10.1029/2004PA001081.

Konovalov, S.K., Ivanov, L.I., Samodurov, A.S., 2000. Oxygen, nitrogen and sulphide fluxes in the Black Sea. Mediterr. Mar. Sci. 1, 41–59. https://doi.org/10.12681/mms.289.

Kouchinsky, A., Bengtson, S., Gallet, Y., Korovnikov, I., Pavlov, V., Runnegar, B., Shields, G., Veizer, J., Young, E., Ziegler, K., 2008. The SPICE carbon isotope excursion in Siberia: a combined study of the upper Middle Cambrian–lowermost Ordovician Kulyumbe River section, northwestern Siberian Platform. Geol. Mag. 145, 609–622. https://doi.org/10.1017/S0016756808004913.

Kuypers, M.M.M., van Breugel, Y., Schouten, S., Erba, E., Sinninghe Damste, J.S., 2004. N_2-fixing cyanobacteria supplied nutrient N for cretaceous oceanic anoxic events. Geology 32, 853–856. https://doi.org/10.1130/G20458.1.

Lenton, T.M., Watson, A.J., 2000. Redfield revisited 1. Regulation of nitrate, phosphate, and oxygen in the ocean. Glob. Biogeochem. Cycles 14 (1), 225–248. https://doi.org/10.1029/1999GB900065.

Lenton, T.M., Daines, S.J., Mills, B.J.W., 2018. COPSE reloaded: an improved model of biogeochemical cycling over Phanerozoic time. Earth Sci. Rev. 178, 1–28. https://doi.org/10.1016/j.earscirev.2017.12.004.

LeRoy, M.A., Gill, B.C., 2019. Evidence for the development of local anoxia during the Cambrian SPICE event in eastern North America. Geobiology 17, 381–400. https://doi.org/10.1111/gbi.12334.

LeRoy, M.A., Gill, B.C., Sperling, E.A., McKenzie, N.R., Park, T.S., 2021. Variable redox conditions as an evolutionary driver? A multi-basin comparison of redox in the middle and later Cambrian oceans (Drumian-Paibian). Palaeogeogr. Palaeoclimatol. Palaeoecol. 566, 110209 https://doi.org/10.1016/j.palaeo.2020.110209.

Li, D., Zhang, X., Hu, D., Chen, X., Huang, W., Zhang, X., Li, M., Qin, L., Peng, S., Shen, Y., 2018. Evidence of a large $\delta^{13}C_{carb}$ and $\delta^{13}C_{org}$ depth gradient for deep-water anoxia during the late Cambrian SPICE event. GSA Bull. 46, 631–634. https://doi.org/10.1130/G40231.1.

Liu, J., Qie, W., Algeo, T.J., Yao, L., Huang, J., Luo, G., 2015. Changes in marine nitrogen fixation and denitrification rates during the end-Devonian mass extinction. Palaeogeogr. Palaeoclimatol. Palaeoecol. 448, 195–206. https://doi.org/10.1016/j.palaeo.2015.10.022.

Mills, B.J.W., Krause, A.J., Jarvis, I., Cramer, B.D., 2023. Evolution of atmospheric O_2 through the Phanerozoic, Revisited. Annu. Rev. Earth Planet. Sci. 51, 253–276. https://doi.org/10.1146/annurev-earth-032320-095425.

Monteiro, F.M., Pancost, R.D., Ridgwell, A., Donnadieu, Y., 2012. Nutrients as the dominant control on the spread of anoxia and euxinia across the Cenomanian-Turonian oceanic anoxic event (OAE2): Model-data comparison. Paleoceanography 27, PA4209. https://doi.org/10.1029/2012PA002351.

Moore, C.M., Mills, M.M., Arrigo, K.R., et al., 2013. Processes and patterns of oceanic nutrient limitation. Nat. Geosci. 6, 701–710. https://doi.org/10.1038/ngeo1765.

Mort, H.P., Adatte, T., Foellmi, K.B., Keller, G., Steinmann, P., Matera, V., Berner, Z., Stueben, D., 2007. Phosphorus and the roles of productivity and nutrient recycling during oceanic anoxic event 2. Geology 35, 483–486. https://doi.org/10.1130/G23475A.1.

Naafs, B.D.A., Monteiro, F.M., Pearson, A., Higgins, M.B., Pancost, R.D., Ridgwell, A., 2019. Fundamentally different global marine nitrogen cycling in response to severe ocean deoxygenation. Proc. Natl. Acad. Sci. 116 (50), 24979–24984. https://doi.org/10.1073/pnas.1905553116.

Palmer, A.R., 1965. Biomere: a new kind of biostratigraphic unit. J. Paleontol. 39, 149–153.

Palmer, A.R., 1984. The biomere problem: Evolution of an idea. J. Paleontol. 58, 599–611.

Peng, S.C., Babcock, L.E., Ahlberg, P., 2020. Chapter 19: The Cambrian Period. In: Gradstein, F.M., Ogg, J.G., Schmitz, M.D., Ogg, G.M. (Eds.), Geologic Time Scale 2020, vol. 2. Elsevier, Amsterdam, pp. 565–629. https://doi.org/10.1016/B978-0-12-824360-2.00011-5.

Pisarzowska, A., Rakociński, M., Marynowski, L., Szczerba, M., Thoby, M., Paszkowski, M., Perri, M.C., Spalletta, C., Schönlaub, H., Kowalik, N., Gereka, M., 2020. Large environmental disturbances caused by magmatic activity during the late Devonian Hangenberg Crisis. Glob. Planet. Chang. 190, 103155 https://doi.org/10.1016/j.gloplacha.2020.103155.

Pohl, A., Ridgwell, A., Stockey, R.G., Thomazo, C., Keane, A., Vennin, E., Scotese, C.R., 2022. Continental configuration controls ocean oxygenation during the Phanerozoic. Nature 608, 523–527. https://doi.org/10.1038/s4156-022-05018-z.

Pruss, S.B., Jones, D.S., Fike, D.A., Tosca, N.J., Wignall, P.B., 2019. Marine anoxia and sedimentary mercury enrichments during the late Cambrian SPICE event in northern Scotland. Geology 47, 475–478. https://doi.org/10.1130/G45871.1.

Robinson, R.S., Kienast, M., Albuquerque, A.L., et al., 2012. A review of nitrogen isotopic alteration in marine sediments. Paleoceanography 27, PA4203. https://doi.org/10.1029/2012PA002321.

Rooney, A.D., Milikin, A.E.G., Ahlberg, P., 2022. Re-Os geochronology for the Cambrian SPICE event: Insights into euxinia and enhanced continental weathering from radiogenic isotopes. Geology 50 (6), 716–720. https://doi.org/10.1130/G49833.1.

Runkel, A.C., McKay, R.M., Palmer, A.R., 1998. Origin of a classic cratonic sheet sandstone: Stratigraphy across the Sauk II–Sauk III boundary in the Upper Mississippi Valley. GSA Bull. 110, 188–210. https://doi.org/10.1130/0016-7606(1998)110<0188:OOACCS>2.3.CO;2.

Runkel, A.C., Miller, J.F., McKay, R.M., Palmer, A.R., Taylor, J.F., 2007. High-resolution sequence stratigraphy of lower Paleozoic sheet sandstones in Central North America: the role of special conditions of cratonic interiors in development of stratal architecture. GSA Bull. 119, 860–881. https://doi.org/10.1130/B26117.1.

Runkel, A.C., McKay, R.M., Cowan, C.A., Miller, J.F., Taylor, J.F., 2012. The Sauk megasequence in the cratonic interior of North America: Interplay between a fully developed inner detrital belt and the central great American carbonate bank. In: Derby, J.R., Fritz, R.D., Longacre, S.A., Morgan, W.A., Sternbach, C.A. (Eds.), The Great American Carbonate Bank: The Geology and Economic Resources of the Cambrian – Ordovician Sauk Megasequence of Laurentia, vol. 98. AAPG Memoir, pp. 1001–1011.

Ruvalcaba Baroni, I., van Helmond, N.A.G.M., Tsandev, I., Middelburg, Slomp, C.P., 2015. The nitrogen isotope composition of sediments from the proto-North Atlantic during Oceanic Anoxic Event 2. Paleoceanography 30, 923–937. https://doi.org/10.1002/2014PA002744.

Saltzman, M.R., 2005. Phosphorus, nitrogen, and the redox evolution of the Paleozoic oceans. Geology 33, 573–576. https://doi.org/10.1130/G21535.1.

Saltzman, M.R., Brasier, M.D., Ripperdan, R.L., Ergaliev, G.K., Lohmann, K.C., Robison, R.A., Chang, W.T., Peng, S., Runnegar, B., 2000. A global carbon isotope excursion during the late Cambrian: Relation to trilobite extinctions, organic-matter burial and sea level. Palaeogeogr. Palaeoclimatol. Palaeoecol. 162, 211–223. https://doi.org/10.1016/S0031-0182(00)00128-0.

Saltzman, M.R., Cowan, C.A., Runkel, A.C., Runnegar, B., Stewart, M.C., Palmer, A.R., 2004. The late Cambrian SPICE ($\delta^{13}C$) event and the SAUK II–SAUK III regression:

new evidence from Laurentian basins in Utah, Iowa, and Newfoundland. J. Sediment. Res. 74, 366–377. https://doi.org/10.1306/120203740366.
Saltzman, M.R., Young, S.A., Kump, L.R., Gill, B.C., Lyons, T.W., Runnegar, B., 2011. A pulse of atmospheric oxygen during the late Cambrian. Proc. Natl. Acad. Sci. 108, 3876–3881. https://doi.org/10.1073/pnas.1011836108.
Schachat, S.R., Labandeira, C.C., Saltzman, M.R., Cramer, B.D., Payne, J.L., Boyce, K., 2018. Phanerozoic pO_2 and the early evolution of terrestrial animals. Proceed. Roy. Soc. Part B 285 (1871), 20172631. https://doi.org/10.1098/rspb.2017.2631.
Schiffbauer, J.D., Huntley, J.W., Fike, D.A., Jeffrey, M.J., Gregg, J.M., Shelton, K.L., 2017. Decoupling biogeochemical records, extinction, and environmental change during the Cambrian SPICE event. Sci. Adv. 6, 1602158. https://doi.org/10.1126/sciadv.1602158.
Schmid, S., Smith, P.M., Woltering, M., 2018. A basin-wide record of the late Cambrian Steptoean positive carbon isotope excursion (SPICE) in the Amadeus Basin, Australia. Palaeogeogr. Palaeoclimatol. Palaeoecol. 508, 116–128. https://doi.org/10.1016/j.palaeo.2018.07.027.
Scotese, C.R., 2014. Atlas of Cambrian and early Ordovician Paleogeographic Maps (Mollweide Projection). In: Maps 81–88, the Early Paleozoic. PALEOMAP Atlas for ArcGIS, PALEOMAP Project, vol. 5. Evanston, IL. https://www.academia.edu/16785571/Atlas_of_Cambrian_and_Early_Ordovician_Paleogeographic_Maps.
Sigman, D.M., Casciotti, K.L., 2001. Nitrogen isotopes in the ocean. In: Steele, J.H., Turekian, K.K., Thorpe, S.A. (Eds.), Encyclopedia of Ocean Sciences. Academic Press, London, pp. 1884–1894. https://doi.org/10.1006/rwos.2001.0172.
Sloss, L.L., 1988. Tectonic evolution of the craton in Phanerozoic time. In: Sloss, L.L. (Ed.), Sedimentary cover—North American craton, United States: Geological Society of America, D-2. Geology of North America, pp. 25–51.
Sproson, A.D., Pogge von Strandmann, P.A.E., Selby, D., et al., 2022. Osmium and lithium isotope evidence for weathering feedbacks linked to orbitally paced organic carbon burial and Silurian glaciations. Earth Planet. Sci. Lett. 577, 117260 https://doi.org/10.1016/j.epsl.2021.117260.
Stolfus, B.M., Allman, L.J., Young, S.A., Calner, M., Hartke, E.R., Oborny, S.C., Bancroft, A.M., Cramer, B.S., 2023. Expansion of reducing environments during the Ireviken Biogeochemical Event: evidence from the Altajme core, Gotland, Sweden. Paleoceanograph. Paleoclimatol. 38 https://doi.org/10.1029/2022PA004484 e2022PA004484.
Taylor, J.F., 2006. History and status of the biomere concept. Memoir. Assoc. Austral. Palaeontol. 32, 247–265.
Turgeon, S.C., Creaser, R.A., 2008. Cretaceous oceanic anoxic event 2 triggered by a massive magmatic episode. Nature 454, 323–326. https://doi.org/10.1038/nature07076.
Tyrrell, T., 1999. The relative influences of nitrogen and phosphorus on oceanic primary production. Nature 400, 525–531. https://doi.org/10.1038/22941.
Van Cappellen, P., Ingall, E.D., 1994. Benthic phosphorus regeneration, net primary production, and ocean anoxia: a model of the coupled marine biogeochemical cycles of carbon and phosphorus. Paleoceanography 9, 677–692. https://doi.org/10.1029/94PA01455.
Voss, M., Bange, H.W., Dippner, J.W., Middelburg, J.J., Montoya, J.P., Ward, B., 2013. The marine nitrogen cycle: recent discoveries, uncertainties and the potential relevance of climate change. Philosoph. Trans. Royal Soc., Part B Biol. Sci. 368, 20130121. https://doi.org/10.1098/rstb.2013.0121.
Wignall, P.B., 1991. Model for transgressive black shales? Geology 19 (2), 167–170. https://doi.org/10.1130/0091-7613(1991)019<0167:MFTBS>2.3.CO;2.
Woods, M.A., Wilby, P.R., Leng, M.J., Rushton, A.W.A., Williams, M., 2011. The Furongian (late Cambrian) Steptoean positive Carbon Isotope Excursion (SPICE) in Avalonia. J. Geol. Soc. Lond. 168, 851–862. https://doi.org/10.1144/0016-76492010-111.
Zhang, X., Gao, Y., Chen, X., Hu, D., Li, M., Wang, C., Shen, Y., 2019. Nitrogen isotopic composition of sediments from the eastern Tethys during Oceanic Anoxic Event 2. Palaeogeogr. Palaeoclimatol. Palaeoecol. 515, 123–133. https://doi.org/10.1016/j.palaeo.2018.03.013.
Zhang, L., Algeo, T.J., Zhao, L., Dahl, T.W., Chen, Z., Zhang, Z., Poulton, S.W., Hughes, N.C., Gou, X., Li, C., 2023. Environmental and trilobite diversity changes during the middle-late Cambrian SPICE event. GSA Bull. https://doi.org/10.1130/B36421.1.
Zhao, Z., Thibault, N.R., Dahl, T.W., Schovsbo, N.H., Sørensen, A.L., Rasmussen, C.M.Ø., Nielsen, A.T., 2022. Synchronizing rock clocks in the late Cambrian. Nat. Commun. 13, 1990. https://doi.org/10.1038/s41467-022-29651-4.
Zhao, Z., Pang, X., Zou, C., Dickson, A.J., Basu, A., Guo, Z., Pan, S., Nielsen, A.T., Schovsbo, N.H., Jing, Z., Dahl, T.W., 2023. Dynamic oceanic redox conditions across the late Cambrian SPICE event constrained by molybdenum and uranium isotopes. Earth Planet. Sci. Lett. 604, 118013 https://doi.org/10.1016/j.epsl.2023.118013.
Zhu, M.Y., Yang, A.H., Yuan, J.L., Li, G.X., Zhang, J.M., Zhao, F.C., 2019. Cambrian integrative stratigraphy and timescale of China. Sci. China Earth Sci. 62, 25–60. https://doi.org/10.1007/s11430-017-9291-0.